Effect of crystal orientation and nanofiller alignment on dielectric breakdown of polyethylene/montmorillonite nanocomposites

Bo Li,[1,2,a)] Panagiotis I. Xidas,[1,3] Kostas S. Triantafyllidis,[3] and Evangelos Manias[1,a)]
[1]*Department of Materials Science and Engineering, The Pennsylvania State University, University Park, Pennsylvania 16802, USA*
[2]*PolyK Technologies, LLC, 2124 Old Gatesburg Road, State College, Pennsylvania 16803, USA*
[3]*Department of Chemistry, Aristotle University of Thessaloniki, Thessaloniki GR 54124, Greece*

(Received 18 July 2017; accepted 16 August 2017; published online 24 August 2017)

Extrusion blown polyethylene and polyethylene/montmorillonite nanocomposite films were cold stretched to various ratios to quantify the influence of the crystal orientation and the nanofiller alignment on their dielectric breakdown performance. It was found that the crystal orientation could increase the breakdown strength (E_{BD}) in the stretched blown films. The aligned pseudo-2D inorganic nanoclays provided additional strong improvements in E_{BD} that can be superimposed to any E_{BD} enhancement due to the polymer crystal orientation. At high filler loadings and high stretching ratios, the onset of percolation was observed through a substantial improvement in the dielectric breakdown strength. *Published by AIP Publishing.* [http://dx.doi.org/10.1063/1.4996717]

Polyethylene (PE) is one of the most commonly used polymer materials as electrical insulators, because of its excellent electrical properties. Ever improving electrical and electronic technologies place a high demand on the performance of the next generation insulators, which should be able to withstand a substantially large electric field, far beyond what can be achievable with the current state of the art.[1,2] Recently, improved electrical properties have been recorded in nanoclay filled polymer composites. These nanocomposites exhibited increased resistance to partial discharges and low charge accumulation, which can eventually lead to enhanced breakdown strength and prolonged service time.[3,4] The improvement was attributed to the high aspect ratio and the platelet shape of the nanoclays, which necessitate a tortuous pathway for electrical treeing propagation around the fillers.[5–8] Other researchers also assigned the improved performance to the filler interfaces,[1,4,6,9] which served as traps for mobile charges, and which could also mitigate charge accumulation if the interfaces with enhanced local conductivity overlapped. Considering the other properties that can be simultaneously improved in these nanoclay composites,[10] polyethylene-nanoclay composites are as one of the most promising dielectric materials for high voltage electrical insulating technologies.

In the past years, most work has been done on the "isotropic" composites with randomly dispersed nanoclays;[1,11] the composites with controlled morphologies are less commonly reported. In our previous work,[5] the PE nanocomposites with aligned nanosilicates demonstrated enhanced dielectric breakdown strength and reduced high field energy loss over their isotropic counterparts. That work also strongly suggested a barrier mechanism to charge treeing as responsible for the improved performance. Here in this letter, we continue to tailor the morphology of these polymers and polymer composites, with the emphasis on the orientation of polymer crystals and of inorganic fillers, to delineate contributions of these two structural alignments on the electrical breakdown properties.

The as-received PE and PE/montmorillonites (MMT) composite films were produced at a commercial blown film line (Pliant Corporation),[5,12] and then cold-stretched to improve the PE crystal orientation. The PE used here is a Dow Integral polyolefin (an 80/20 blend of linear low density PE/low density PE). The layered-silicates were commercial organo-montmorillonites (o-MMT) from Nanocor, with a cation exchange capacity of 1.0 meq/g, organically modified by dimethyl-dioctadecyl-ammonium surfactants. The o-MMT were first dispersed at 25 wt. % inorganic loading with a twin-screw extruder in a maleic anhydride functionalized PE (PE-Mah with 0.26 wt. % Mah grafting density, $\overline{M}_w = 67\,000$ g mol^{-1}, and $\overline{M}_w/\overline{M}_n = 6.1$), then diluted by PE to achieve a final o-MMT concentration of 6 wt. % and 9 wt. %, respectively, and finally blown into the as-received films. The unfilled PE films were produced under the same conditions. These films were cut into 5–10 cm wide strips, which were stretched along the machine direction by an Instron 5566 tensile apparatus at room temperature. The strain rates were set at 10 mm/min for the composite and 15 mm/min for the polymer in order to maintain uniform deformation.

Transmission electron microscopy (TEM, Jeol JEM-2010 with LaB_6 emitter) was performed at an accelerating voltage of 200 kV on composite films microtomed by a Leica Ultracut UCT Microtome with cryoattachment. The transmission-mode wide-angle X-ray diffraction (WAXD) was done in a Rigaku D/MAX Rapid II instrument equipped with a 2D-detector and a graphite monochromator, using a 100 μm pinhole collimator, a 127.4 mm sample-to-detector distance, and Cu K$\alpha_{1,2}$ radiation (weighted average $\lambda = 1.5418$ Å). The films were measured with the X-ray beam normal to the film surface (face-on) or parallel to the film surface (edge-on). One dimensional (1D) WAXD profiles were obtained by integrating the corresponding two dimensional (2D) WAXD images. Differential scanning calorimetry (DSC) was carried out in a Thermal Analysis Instruments Q100 calorimeter operated at

[a)]Authors to whom correspondence should be addressed: bolipsu@gmail.com and manias@psu.edu

heating and cooling temperature ramps of 10 °C/min under a nitrogen atmosphere. Dielectric breakdown measurements were performed on a TREK P0621P instrument. The samples were sandwiched between a one-side conducting polypropylene tape (top electrode) and a copper plate (bottom electrode). All specimens were tested under a dc voltage ramp of 500 V/s (more details can be found in Refs. 5 and 13).

The dispersion and morphology of MMT nanofillers in the PE composites can be directly observed by TEM and further assessed by XRD. Figure 1(a) presents the TEM image and the 2D XRD (edge-on) of the as-received composite film with 6 wt. % o-MMT. At the μm scale, clay tactoids consisting of a few layers down to a single layer are uniformly dispersed in the PE matrix. A preferential filler orientation along the flow direction can also be identified, which corresponds to the azimuthal narrowing of the diffraction bands from MMT in the inset XRD graph. The filler orientation, induced by the blowing manufacturing, is largely retained in the as-received composite films, as the μm-scale lateral dimension of the clay prevents its rearrangement during the subsequent polymer relaxation and crystallization. As shown in Fig. 1(b), at the nm scale, the organoclays are intercalated by the polymer, with the intergallery spacing expanding to 46 Å ($2\theta_{\text{MMT-001}} \approx 1.9°$). The locally intercalated structure implies thermodynamically favorable mixing, which originates from the intentionally introduced Mah groups, i.e., the increased interaction between the Mah and MMT surfaces compensates the reduced entropy of the intercalated polymer chains.[14]

It is known that the crystal orientation and crystallization are usually accompanied with the cold-stretching. As a result, the crystallinity of all films is measured from the first melting enthalpy by DSC in order to evaluate the strain-induced crystallization; and 2D-XRD is employed to quantify the crystal orientation. Figure 2 shows the crystallinity change with stretching for all films. The expected strain-induced crystallization is greatly limited (the crystallinity increases by less than 4% for each system over the entire strain range); and the difference in crystallinity between the various systems is less than 3% across all specimen films at certain strains. These results are not surprising, as the polymer matrix is highly nucleated, which already maximizes the crystal fraction, even before the MMT addition and the uniaxial stretching.

The strain-induced crystal orientation can be directly perceived by the azimuthally narrowed diffraction rings for

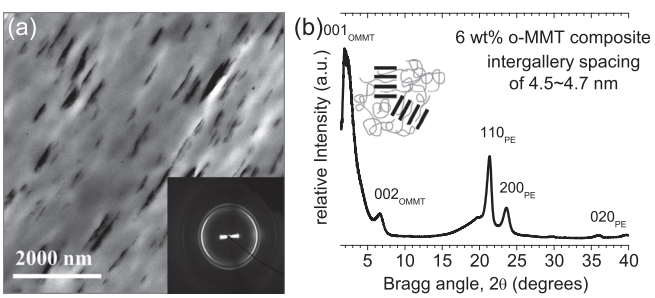

FIG. 1. (a) TEM image of the as-received 6 wt. % composite film (inset: 2D XRD pattern recorded on the same film). (b) 1D XRD pattern of the 6 wt. % nanocomposite film, obtained by integrating 2D XRD azimuthally.

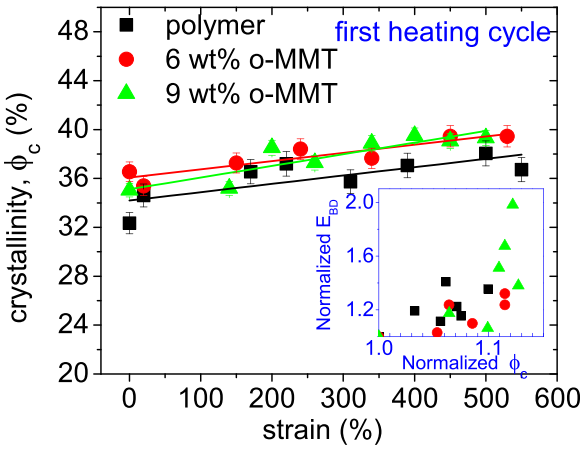

FIG. 2. Crystallinity vs. strain for all films (inset: normalized breakdown strength vs. normalized crystallinity).

PE crystals (the two bright rings correspond to PE 110 and 200 planes, respectively), as shown in the top panel of Fig. 3. Quantitatively, the order parameters (S_d) for specific diffraction peaks are calculated by Hermans orientation function

$$S_d = \frac{3\langle\cos^2\phi\rangle - 1}{2} \text{ with } \langle\cos^2\phi\rangle = \frac{\int_0^{\pi/2} I(\phi)\cos^2\phi\sin\phi d\phi}{\int_0^{\pi/2} I(\phi)\sin\phi d\phi}. \quad (1)$$

$I(\phi)$ are radial intensities; the radial ϕ is defined as $\cos(\phi) = \cos(\beta)\cos(\theta)$, with β being the azimuthal angle and θ being the usual Bragg angle. The order parameter is calculated for any diffraction peak (hkl) given its background-corrected azimuthal intensities $I(\beta)$ which were then converted to radial

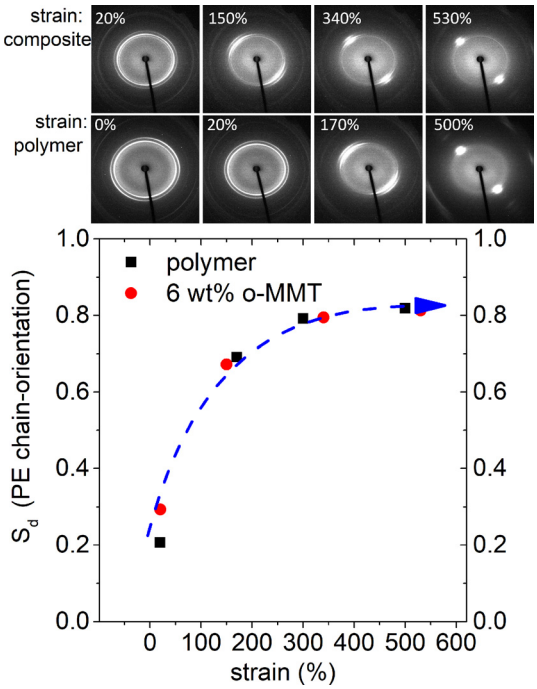

FIG. 3. (Top) 2D XRD patterns of the polymer and of the 6 wt. % composite films with increased strains. (Bottom) Order parameter of polymer chain orientation vs. strain.

intensities I(ϕ). $S_d = 0$ denotes a randomly oriented *hkl* plane; $S_d = -0.5$ a plane oriented along the reference axis (symmetry axis); whereas $S_d = 1$ a plane perfectly perpendicular to the reference axis. Since the stretched sample films exhibit a fiber symmetry with polymer chains aligned along the strain direction, the chain orientation should be evaluated to compare the crystal orientation extent of the samples. According to polymer crystallography, the lamellae surfaces (00l) are perpendicular to the chain direction, which are absent in the 2D XRD patterns here. However, for the orthorhombic PE crystal structure, the order parameter of (00l) planes can be calculated from the (200) and (110) diffracted peaks as usual[15]

$$\langle \cos^2\phi \rangle_{00l} = 1 - 0.555\langle \cos^2\phi \rangle_{200} - 1.445\langle \cos^2\phi \rangle_{110}, \quad (2)$$

where $\langle \cos^2\phi \rangle_{200}$ and $\langle \cos^2\phi \rangle_{110}$ are the orientation parameters for PE (200) and (110) planes, respectively [Eq. (1)]. The order parameters (S_d) for chain orientation are plotted in Fig. 3. The strain induced orientation can be identified in both polymers and composites. The monotonic, albeit nonlinear, increase in orientation with strains corresponds to an intralamellar chain slip towards the formation of fibrillar structure, both of which are irreversible deformation occurring after yield point.[16] Interestingly, the organoclay nanofillers do not alter this chain orientation, as evidenced by the similar order parameters and trends between the polymer and composite films, therefore, allowing the use of the strain value as a measure of crystal orientation for both unfilled PE films and composites (Fig. 4). By the same approach, the orientation of the nanoclays in the as-received composite films are also calculated from the respective 2D XRD patterns (e.g., inset of Fig. 1), with $S_d = 0.8$–0.9 for these nanofillers ($S_d = 1$ means the perfect alignment), which is consistent with the direct TEM observation that most nanoclays are already highly oriented in these composites, even before the stretching.

The dielectric breakdown strengths of all films are calculated through the framework of Weibull statistics[17] from the distribution of experimentally observed breakdown electric fields (E) (see supplementary material for the Weibull plots of all films)

$$P(E_{BD}, \beta_w, E) = 1 - \exp\left(-\left(\frac{E}{E_{BD}}\right)^{\beta_w}\right). \quad (3)$$

E_{BD} is the characteristic breakdown strength, defined as the electric field under which the failure probability (P) accumulates to 63.2%; and the Weibull modulus (β_w) quantifies the scattering for experimental data. Figure 4(a) compares E_{BD} values at different strains for all films. The strain-induced increase in E_{BD} can be identified in all films, which should be related to the crystal orientation. The small variation in crystallinity cannot be regarded as the dominant factor. In fact, as shown in the inset of Fig. 2, in which the normalized E_{BD} is plotted as a function of the normalized crystallinity, no clear correlation can be established. The E_{BD} improvement with crystal orientation is in agreement with the typical behavior of oriented semicrystalline polymer films,[5,18,19] as the oriented crystallites provide more barriers and necessitates more tortuous pathways for electrical treeing around them.[19] It can also be observed that the nanocomposites exhibit a larger breakdown strength than the unfilled polymers.

The influence of the crystal orientation and the aligned nanoclays on the dielectric breakdown performance is further quantified from the normalized curves as shown in Fig. 4(b). For the polymer and the 6 wt. % nanocomposite, a great overlap between their normalized E_{BD} curves is consistent with their overlapped crystal orientation plots (Fig. 3), suggesting that the same orientation of PE crystallites provides an identical E_{BD} enhancement in these two films, regardless of with or without fillers. The incorporation of oriented nanofillers offers an additional increase in E_{BD}, which is almost constant over the entire strain [ca. 100 MV/m, Fig. 4(a)]. This can be understood because the aligned 2D nanoclays, similar to the oriented crystals, can also increase the path tortuosity for electrical treeing;[5,8] besides, these nanofillers are already highly aligned in the non-stretched composite films, leaving less room for the further orientation with stretching. This behavior denotes that an additional amount of barriers, which are associated with the aligned fillers and which are nearly independent of strain, is superposed to the oriented polymer crystal effect in a straightforward manner, a supposition which is also supported by the comparable β_w values for the two sets of films [Fig. 4(a)]. For the higher filler concentration, the 9 wt. % composite begins with a similar breakdown performance to the other two films up to a strain of ca. 260% [Fig. 4(b)]. Upon crossing that strain, the normalized E_{BD} curve deviates from the shape of the unfilled PE and the low filler loading composite, exhibiting a substantially large and strain-dependent increase. Finally, a twofold increase in E_{BD} can be achieved at the strain of 500%. This higher-than-expected enhancement indicates the percolation of fillers and polymer crystals, i.e., the gradually oriented crystals eventually establish a macroscopic barrier

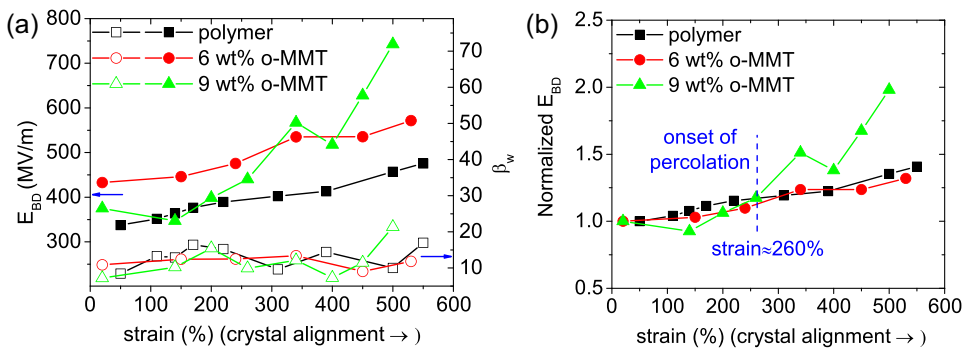

FIG. 4. (a) Weibull breakdown strength (E_{BD}) and Weibull modulus (βw) vs. strain for all films. (b) Normalized E_{BD} (with respect to the first low-strain breakdown point in each film) vs. strain.

structure, along with the aligned nanofillers, leading to a substantially increased E_{BD}.

In summary, polymer crystals were systematically oriented in PE and PE/MMT nanocomposites to study the effect of crystal orientation and pseudo-2D nanofiller alignment on the breakdown strength. Crystal orientation could improve E_{BD}, to the same extent in the unfilled PE and PE composites. Incorporation of oriented fillers provided an additional non-trivial increase in E_{BD}, synergistically added to any contribution from crystal orientation. At a low filler loading, this increase was nearly constant over the strains; at a high filler loading, a pronounced increase was identified at high strains, suggesting the formation of macroscopic barriers.

See supplementary material for the Weibull plots of all films.

Financial support from the National Science Foundation, as part of the Center for Dielectrics and Piezoelectrics under Grant Nos. IIP-1361571 and IIP-1361503 is acknowledged. Additional support through CSC and ΓΓΕΤ fellowships is acknowledged by B.L. and P.I.X., respectively.

[1]T. Tanaka, IEEE Trans. Dielectr. Electr. Insul. **12**(5), 914 (2005).
[2]C. Yang, P. C. Irwin, and K. Younsi, IEEE Trans. Dielectr. Electr. Insul. **11**(5), 797 (2004).
[3]T. Imai, F. Sawa, T. Nakano, T. Ozaki, T. Shimizu, M. Kozako, and T. Tanaka, IEEE Trans. Dielectr. Electr. Insul. **13**(2), 319 (2006); J. K. Nelson, *Dielectric Polymer Nanocomposites* (Springer, New York, NY, 2010); M. Kozako, N. Fuse, Y. Ohki, T. Okamoto, and T. Tanaka, IEEE Trans. Dielectr. Electr. Insul. **11**(5), 833 (2004).
[4]R. Smith, C. Liang, M. Landry, J. Nelson, and L. Schadler, IEEE Trans. Dielectr. Electr. Insul. **15**(1), 187 (2008); M. Roy, J. K. Nelson, R. K. MacCrone, and L. S. Schadler, J. Mater. Sci. **42**(11), 3789 (2007).
[5]V. Tomer, G. Polizos, C. A. Randall, and E. Manias, J. Appl. Phys. **109**(7), 074113 (2011).
[6]M. G. Danikas and T. Tanaka, IEEE Electr. Insul. Mag. **25**(4), 19 (2009).
[7]C. Green and A. Vaughan, IEEE Electr. Insul. Mag. **24**(4), 6 (2008); T. Tanaka, G. C. Montanari, and R. Mulhaupt, IEEE Trans. Dielectr. Electr. Insul. **11**(5), 763 (2004).
[8]S. P. Fillery, H. Koerner, L. Drummy, E. Dunkerley, M. F. Durstock, D. F. Schmidt, and R. A. Vaia, ACS Appl. Mater. Interfaces **4**(3), 1388 (2012).
[9]T. Tanaka, M. Kozako, N. Fuse, and Y. Ohki, IEEE Trans. Dielectr. Electr. Insul. **12**(4), 669 (2005).
[10]A. B. Morgan and C. A. Wilkie, *Flame Retardant Polymer Nanocomposites* (Wiley, Hoboken, NJ, 2007), p. 31.
[11]K. S. Shah, R. C. Jain, V. Shrinet, A. K. Singh, and D. P. Bharambe, IEEE Trans. Dielectr. Electr. Insul. **16**(3), 853 (2009); C. D. Green, A. S. Vaughan, G. R. Mitchell, and T. Liu, *ibid*. **15**(1), 134 (2008).
[12]J. Zhang, E. Manias, G. Polizos, J.-Y. Huh, A. Ophir, P. Songtipya, and M. del M. Jimenez-Gasco, J. Adhes. Sci. Technol. **23**(5), 709 (2009).
[13]V. Tomer and C. A. Randall, J. Appl. Phys. **104**(7), 074106 (2008); V. Tomer, E. Manias, and C. A. Randall, *ibid*. **110**(4), 044107 (2011).
[14]R. A. Vaia and E. P. Giannelis, Macromolecules **30**(25), 7990 (1997).
[15]Z. W. Wilchinsky, J. Polym. Sci., Part A-2: Polym. Phys. **6**(1), 281 (1968).
[16]P. B. Bowden and R. J. Young, J. Mater. Sci. **9**(12), 2034 (1974); K. Sasaguri, S. Hoshino, and R. S. Stein, J. Appl. Phys. **35**(1), 47 (1964); T. An Huy, T. Luepke, and H.-J. Radusch, J. Appl. Polym. Sci. **80**(2), 148 (2001).
[17]W. Weibull, J. Appl. Mech. **18**, 293 (1951).
[18]K. Yahagi, IEEE Trans. Electr. Insul. **EI-15**(3), 241 (1980).
[19]N. Hozumi, M. Ishida, T. Okamoto, and H. Fukagawa, IEEE Trans. Electr. Insul. **25**(4), 707 (1990); T. Tanaka, T. Okamoto, N. Hozumi, and K. Suzuki, IEEE Trans. Dielectr. Electr. Insul. **3**(3), 345 (1996).